



Thickness and sp^3 bond modulation of (Ti/tetrahedral amorphous carbon)_n multilayer coatings

Zhi-Jun Xie¹ · Jia-Lin Li¹ · Ling Gong¹ · Xiang-Li Zhong¹ · Hong-Jia Song¹ · Jin-Bin Wang¹

Received: 10 April 2024 / Revised: 3 June 2024 / Accepted: 17 June 2024
© Youke Publishing Co., Ltd. 2024

Abstract

The durability of wear-resistant tetrahedral amorphous carbon (ta-C) coatings is intimately linked to their thickness and the concentration of sp^3 bonds. To enhance the lifespan of the coatings, we have prepared a multilayer coating consisting of alternating layers of Ti and ta-C, denoted as (Ti/ta-C)_n, using arc ion plating. A multi-layer structure in conjunction with stage cooling is employed to enhance the thickness and promote sp^3 bonding. The results indicate that the I_D/I_G value, representing the ratio of the intensity of the D peak to that of the G peak in Raman spectroscopy, decreases from 0.85 when no stage cooling is applied to 0.35 when stage cooling is employed, suggesting an enhancement in the fraction of sp^3 bonds within the coating. The obtained (Ti/ta-C)_n multilayer coating without peeling off has a maximum thickness of 1.14 μm , which is almost double that of the ta-C coating single layer coating. At the same time, the coating has a low coefficient of friction, down to 0.069, and maintains excellent friction properties with a wear rate of $3.4 \times 10^{-6} \text{ mm}^3 \cdot \text{N}^{-1} \cdot \text{m}^{-1}$. The results conclusively show that the preparation technology can enhance both thickness and sp^3 bonding in ta-C coatings, significantly expanding their utility across tools, molds, and precision engineering components.

Keywords Ta-C coating · Multilayer structure · Arc ion plating · sp^3 bond · Wear resistance

1 Introduction

Tetrahedral amorphous carbon (ta-C) coating is widely utilized in tools, molds, and precision engineering components due to its exceptional hardness, chemical stability, low friction, and wear resistance [1–7]. On the one hand, the higher the content of the sp^3 hybrid bond in the ta-C coating, the better the hardness and wear resistance of the coating [8]. Additionally, the sp^3 hybrid bond content frequently exceeds 50 at.% within ta-C coatings [9]. The temperature at which the material is prepared significantly impacts the proportion of sp^3 bonds present. As temperatures rise, the sp^3 bonds undergo a conversion to sp^2 bonds, subsequently weakening the coating's mechanical characteristics [10]. Consequently,

maintaining a low deposition temperature during the preparation of ta-C coatings is vital for increasing the sp^3 bond content and subsequently enhancing the coating's mechanical properties. However, there are very few studies that focus on controlling the temperature during the deposition process to increase the amount of sp^3 hybrid bonds in ta-C coatings.

On the other hand, the thick ta-C coating has a longer service life than the thin one in the application of wear resistance [11]. However, the thickness of the ta-C coating deposited by physical vapor deposition (PVD) is limited to the significant residual compressive and thermal stresses, which will reduce the bonding strength between the coating and the substrate [12–15]. Excessive thickness of the coating can lead to detachment from the substrate. Notably, in the context of nitride coatings, employing a multilayer structure has been proven to not only mitigate internal stress but also significantly enhance both the hardness and toughness of the coating [16–19]. In the diamond-like carbon (DLC) coating, Sui et al. demonstrate that the CrN/DLC/Cr-DLC multilayer coating can approach micron-scale thickness using imbalanced magnetron sputtering, and the tribological characteristics of the coating are greatly enhanced [20]. The adoption of the WC/DLC multilayer structural design further enhances

✉ Hong-Jia Song
hjsong@xtu.edu.cn

✉ Jin-Bin Wang
jbwang@xtu.edu.cn

¹ National-Provincial Laboratory of Special Function Thin Film Materials, School of Materials Science and Engineering, Xiangtan University, Xiangtan 411105, China

the hardness and wear resistance of the coating [21]. It is widely speculated that a multilayer structure presents itself as a promising avenue for mitigating the stress challenges inherent in ta-C coatings. Nevertheless, the research landscape remains relatively barren, with few studies dedicated to exploring the properties of multilayered ta-C coatings deposited through PVD techniques.

As a PVD method, arc ion plating efficiently deposits ta-C coatings, exhibiting rapid deposition, high energy utilization, a high degree of ionization, and ensuring strong bonding between coatings and substrates [22, 23]. It is suitable for preparing multilayer coatings and can easily control the deposition temperature of the coatings. In this paper, (Ti/ta-C)_n multilayer coatings, where ‘n’ denotes the number of repetitions of the Ti/ta-C bilayer and specifically, featuring a thickness exceeding 1 μm and a high concentration of sp³ bonds, were prepared using arc ion plating. Subsequently, the hardness, friction, and wear resistance properties of these coatings were studied.

2 Experimental

2.1 Coating preparation

Using arc ion plating, ta-C coatings and (Ti/ta-C)_n multilayer structural coatings, in this study, $n = 4$ for comparison with other structures, were deposited onto WC-6 wt.% Co (85HRC 15 mm × 10 mm × 5 mm) cemented carbide substrates, Si substrates, and WC-Co milling cutter. WC-6 wt.% Co has high hardness, excellent wear resistance, and a low friction coefficient, making it suitable for a wide range of demanding coating applications [24]. Before deposition, the substrates were cleaned by ultrasonic for 15 min with acetone solution, then by ultrasonic for 15 min with ethanol solution. Finally, the substrates were dried with nitrogen. Ti target and C target were used in the coating preparation experiment. The whole process was divided into two stages:

substrate etching and coating preparation. The base pressure was maintained at 7×10^{-3} Pa. In the etching stage, Ar⁺ was used to bombard the substrates for 30 min to remove the impurity particles on the substrate surface. Then, the coating was deposited. Before the ta-C coatings and the (Ti/ta-C)_n multilayer structural coatings were deposited, a layer of pure metal Ti was first deposited to improve the bonding strength between the coatings and the substrates. In this study, four types of ta-C coatings and the (Ti/ta-C)_n multilayer structural coatings were deposited. For convenience, in this paper, ta-C deposition 60 min coating with non-stage cooling, ta-C deposition 60 min coating with stage cooling, ta-C deposition 90 min coating with stage cooling, and the (Ti/ta-C)_n multilayer coating with stage cooling are named S₆₀, S_{60C}, S_{90C}, and S_{120C-Ti}, respectively. Figure 1a is a schematic diagram of the vacuum chamber structure of arc ion plating. Our equipment was equipped with thermocouples beside the samples that can be used to check the real-time temperature of the chamber. Our equipment has four sets of targets, which are equipped with Ti, Cr, Ti, and C targets. MS1 and MS2, as indicated in the top-down view of the deposition equipment, represent two positions of unbalanced magnetron sputtering sources. Figure 1a prominently displays an identification marker for Gas ion source (GIS), clearly pinpointing the location of the gas ion source. Moreover, the notation ‘1 rpm’ within the figure designates the rotational velocity of the turntable that supports the sample. Figure 1b is a schematic diagram of (Ti/ta-C)_n multilayer coating structure. Table 1 displays the preparation parameters of the coatings. During the deposition process, the sample utilizing stage cooling maintains a temperature that does not exceed 80 °C, whereas the sample without stage cooling exceeds 150 °C.

2.2 Microstructure characterization

Using a scanning electron microscope (SEM, TESCAN MIR4 LMH, Czech Republic), the coating’s thickness and cross-sectional structure were examined. X-ray diffraction

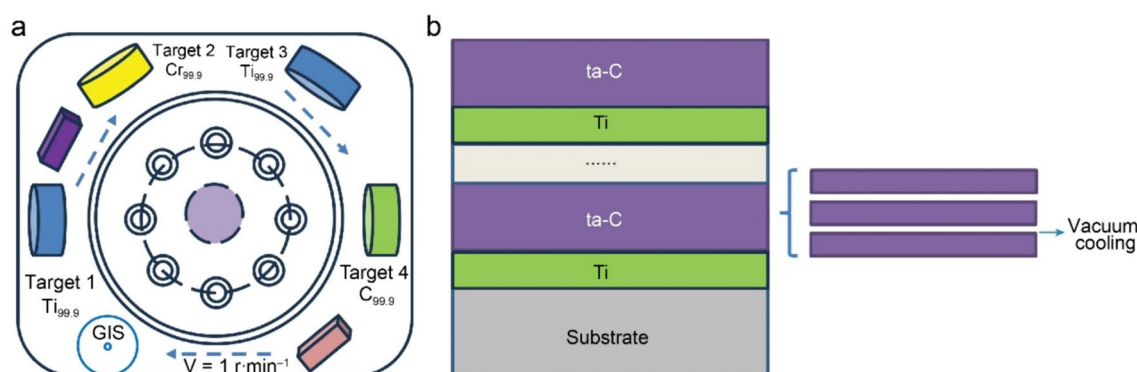


Fig. 1 Schematic illustration of vacuum chamber structure in top view and **b** the diagram of (Ti/ta-C)_n coatings

Table 1 Deposition parameters of ta-C coatings and (Ti/ta-C)_n multilayer coatings

Deposition parameters	Targets	Coatings			
		S ₆₀	S _{60C}	S _{90C}	S _{120C-Ti}
Bias voltage /V	Ti/C targets	-80/-110			
Arc current /A		60/40			
Ion source /kW		0/1			
Deposition time /min		10/60	10/60	10/90	(10/30) ₄

(XRD, Bruker D8 advance, Germany) was used to study the crystal structure using Cu K_{α1} radiation ($\lambda = 0.1541862$ nm) operating at 40 kV and 40 mA. The step scan and scan rate were 0.02° and 5°·min⁻¹, respectively. Thermo Fisher Scientific dxr3 detects the Raman (InVia, Renishaw, UK) signal. The resolution is 0.964 cm⁻¹, and the excitation wavelength is 532 nm. The Vickers hardness of the coating was tested with a micro-Vickers hardness tester (EVERONE MH-500, China), and the average values of five points for each sample were taken. The test parameters are as follows: the test load is 25 g, and the holding time is 15 s.

The HSR-2M (Lanzhou Zhongke Kaihua Technology Co., Ltd, China) high-speed reciprocating friction and wear tester measures the friction coefficient. The specific experimental parameters entailed a test load of 250 g, a reciprocating stroke length of 5 mm, an operating speed of 250 rpm,

and a test duration of 30 min. The friction pair consisted of an Al₂O₃ ceramic disk with a diameter of 10 mm. The entire experiment was conducted using a single sample at room temperature, with each test being repeated three to five times to ensure consistency and reliability of the results.

3 Results and discussion

3.1 Microstructure analysis

As illustrated in Fig. 2, the cross-sectional morphology of the coating was examined using a SEM. The figure indicates that the interface between the coatings is visible. The thickness of ta-C coatings with stage cooling and non-stage cooling is 450 and 460 nm, respectively, as shown in Fig. 2a, b, which demonstrates that the thickness of the coating is not significantly affected by the stage. The thickness of the ta-C coating deposited in 90 min increases to 650 nm, as shown in Fig. 2c. This indicates that the coating thickness increases as the deposition time increases. This may be due to an increase in coating thickness, which leads to higher internal stresses and greater distortion of the hybridized bonds, resulting in increased hardness. However, parts of the S_{90C} coating peel off from the milling cutter, as shown in the inset of Fig. 2c, which is primarily due to the relatively poor adhesion between the coating and the substrate caused

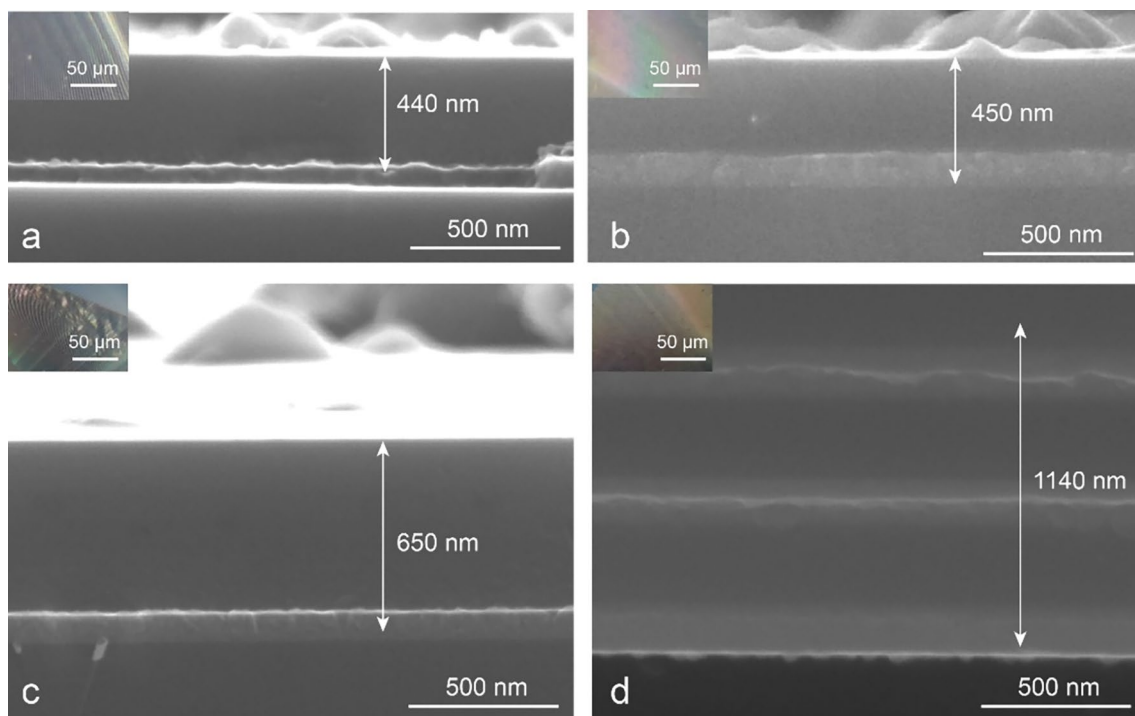


Fig. 2 Cross-section SEM images of ta-C/Ti coating on Si substrate: **a** S₆₀, **b** S_{60C}, **c** S_{90C}, **d** S_{120C-Ti}. Insets show the optically enlarged photograph of ta-C/Ti coating on the WC-Co milling cutter

by the increase in coating thickness and the accumulation of internal stress [11]. Therefore, we prepared the Ti/ta-C four-cycle multilayer coating depicted in Fig. 2d to release the internal stress of the thick ta-C coating. The thickness of the $S_{120C-Ti}$ rose to 1140 nm, and there are no peelings from the milling cutter, as shown in the inset of Fig. 2d, indicating that the multilayer structure of $(Ti/ta-C)_n$ is an effective mean to solve the stress issue in ta-C coatings. The interfaces between layers of a multilayer structure effectively prevent slippage and enhance the overall hardness of the coatings, contributing to their durability.

Figure 3 displays the XRD spectra of the coatings. In Fig. 3, the two diffraction peaks correspond to Si and Ti, respectively. The Si base peak is shown in red on the left, while the Ti diffraction peak is depicted in blue on the right. And there is no C diffraction peak seen in the ta-C coating and the $(Ti/ta-C)_n$ multilayer coating. Therefore, carbon should exist in an amorphous form in coatings.

Figure 4 shows the fitting results of Raman spectra of ta-C coating, and we can find that the curves and the fitted peaks can be well overlapped. Figure 4 shows the Raman spectra of ta-C coating and $(Ti/ta-C)_n$ multilayer coating, reflecting the sp^3 bond content of the coatings under different deposition conditions. From Fig. 4, we can observe that the D peak and G peak of the coatings consistently manifest within the ranges of 1350–1380 and 1550–1570 cm^{-1} , respectively. These positions align precisely with those expected in the standard Raman spectrum of graphite, indicating the presence of characteristic carbon bonding structures [25]. The G peak mainly reflects the information about the sp^2 bond, while the D peak reflects the information about the sp^2 hybrid bond angle disorder, which can be used to explain the existence of fine-grain graphite. The ratio of the D peak intensity to the G peak intensity, I_D/I_G , is mainly used to represent the number and size of the structure of sp^2 rings. The ratio of the peak intensity of D peak to G peak is often used to approximate the content of the sp^3 bond in the

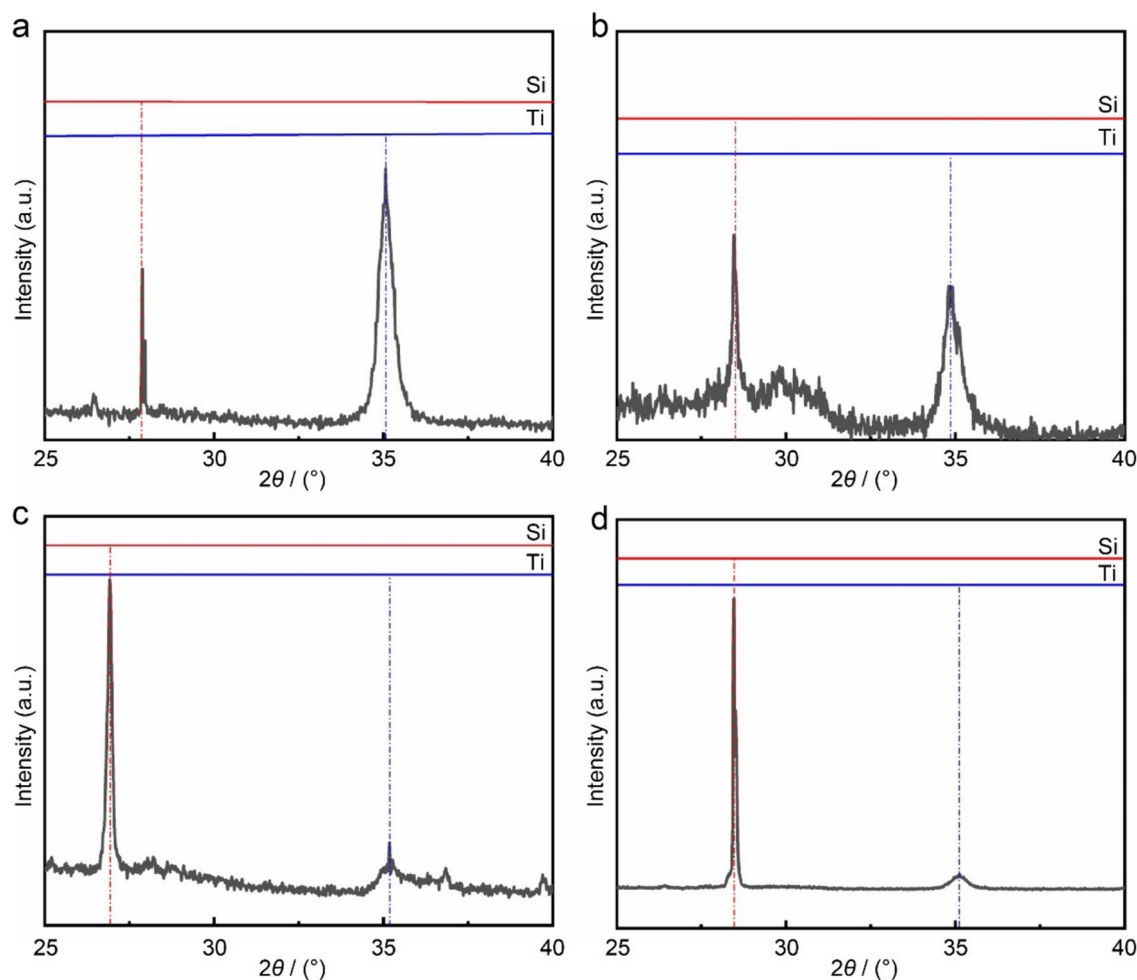


Fig. 3 XRD patterns of ta-C coatings on silicon wafer: **a** S_{60} , **b** S_{60C} , **c** S_{90C} , **d** $S_{120C-Ti}$

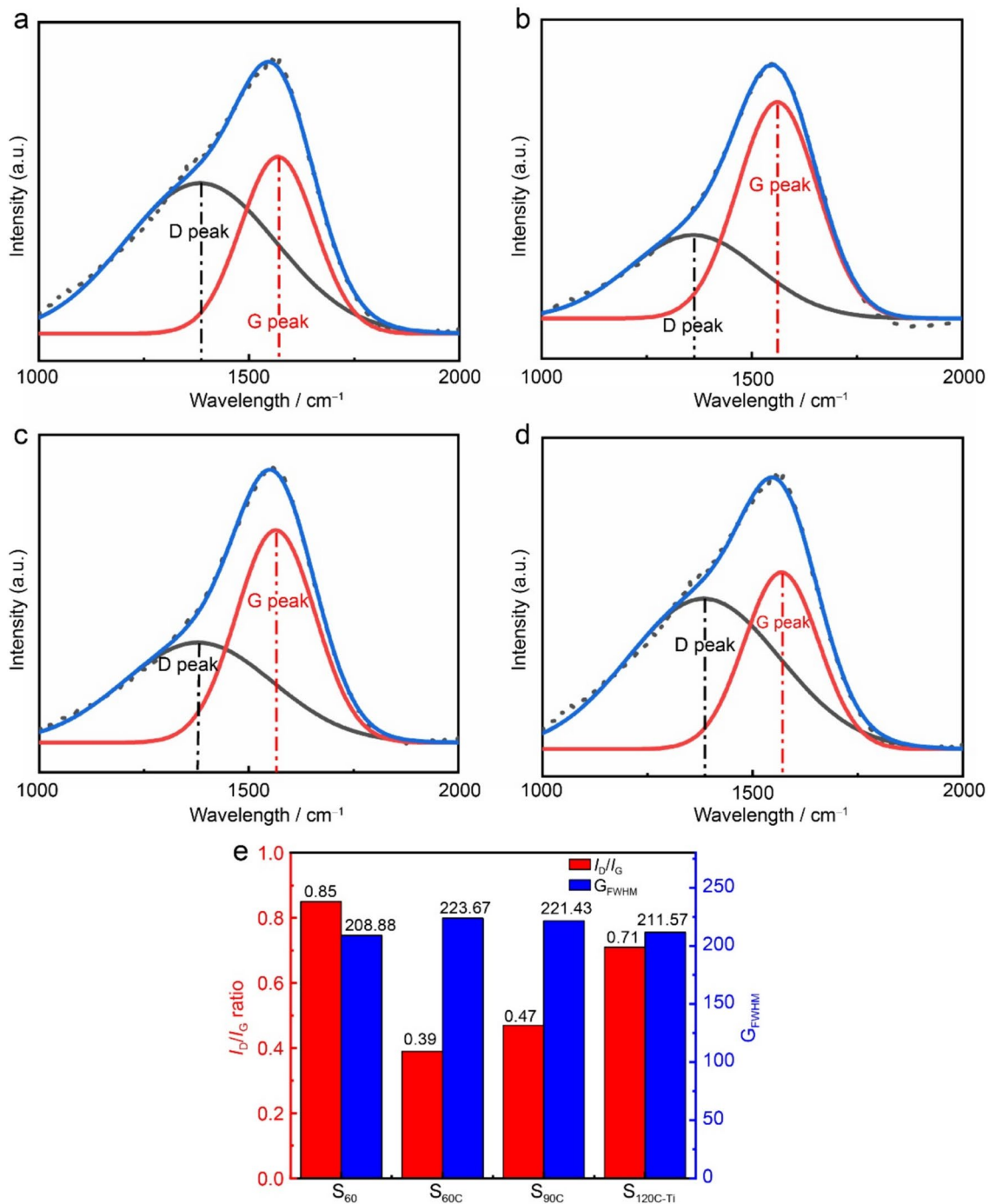


Fig. 4 Raman spectra of the ta-C coatings: **a** S_{60} , **b** S_{60C} , **c** S_{90C} , **d** $S_{120C-Ti}$ and the fitting result of Raman spectra of the ta-C coatings: **e** I_D/I_G ratio and G_{FWHM}

coating. The smaller the value is, the higher the content of the sp^3 bond is [25]. The content of sp^3 hybrid bonds in ta-C coatings increases, and their overall mechanical properties, notably in terms of hardness and durability, become increasingly similar to those of natural diamonds, thereby significantly enhancing their wear resistance [26]. The variation

in the full width at half maximum of the G peak (G_{FWHM}) serves as an indicator, to a certain extent, of the degree of disorder within ta-C coatings. As this value increases, it signifies an escalation in the level of disorder, which can be inferentially linked to changes in the internal stress within the coating, suggesting a corresponding increase in stress

levels. Figure 4e shows the results of the fitting of the ta-C coated Raman spectra I_D/I_G values and G_{FWHM} . From Fig. 4, we can find that the I_D/I_G value of S_{60C} is much smaller than that of S_{60} , which indicates that stage cooling can largely enhance the sp^3 bond content of ta-C coatings. An elevated sp^3 bond content in the coating may yield notable improvements in its mechanical properties, specifically enhancing both its hardness and wear resistance. The I_D/I_G value of S_{90C} , which stands at 0.47, exhibits an increase when compared to that of S_{60C} . This increase can be attributed to the direct correlation between deposition time and temperature during the coating process. As deposition time increases, so does the temperature, triggering a transformation within the coating. Specifically, some of the sp^3 bonds within the coating convert into sp^2 bonds. This chemical transformation, in turn, results in a slight elevation of the I_D/I_G value [10]. However, despite this increase, the I_D/I_G value of S_{90C} remains significantly lower than that of S_{60} . Notably, the I_D/I_G value of the $S_{120C-Ti}$ coating undergoes a rapid elevation to 0.71, accompanied by a decrease in the sp^3 bond content within the coating. This phenomenon is primarily attributed to the enhanced Ti content in the multilayer structure, which subsequently leads to a reduction in the sp^3 bond content of the coating [27]. The G_{FWHM} of the S_{60C} coating, which is 223.67, is the highest, suggesting the greatest internal structural disorder and the highest sp^3 bond content. However, despite its high G_{FWHM} , the thinness of the S_{60C} coating prevents the occurrence of coating spalling. The G_{FWHM} of S_{90C} coating is 221.43, which is slightly lower than that of S_{60C} , but due to its larger thickness and disordered internal structure, the coating accumulates a large number of internal stresses, which results in the phenomenon of peeling of the coating from the milling cutter substrate.

3.2 Mechanical properties

Figure 5 shows the microhardness values of ta-C coating and $(Ti/ta-C)_n$ multilayer coating measured by the micro-Vickers hardness tester. S_{60C} has a microhardness of 3640.6 HV, which is greater than that of S_{60} (3223.8 HV). This is attributed to the stage cooling process of S_{60C} , which lowers the deposition temperature of the coating, thereby facilitating the formation of sp^3 bonds. This, in turn, results in improved hardness, friction resistance, and other mechanical properties. Consequently, the stage cooling process effectively controls the deposition temperature, enabling the preparation of coatings with enhanced hardness [28]. The hardness of S_{90C} is 3829.8 HV. It can be seen from Fig. 4 that the sp^3 bond content of S_{90C} is lower than that of S_{60C} , but its hardness is higher than that of S_{60C} . The primary factor contributing to this phenomenon is the S_{90C} coating's thickness, which attains an impressive 650 nm. With this increased thickness, the number of interfaces is reduced, and the residual

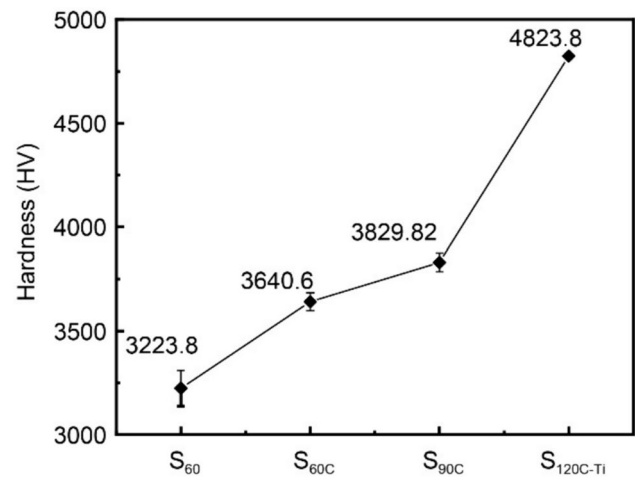


Fig. 5 Microhardness results of ta-C coatings

stress within the coating is heightened, ultimately leading to a notable enhancement in its hardness [29]. This corresponds to the previous thickness analysis in the SEM images of Fig. 2. The hardness of $S_{120C-Ti}$ is the highest, reaching 4823.8 HV, owing primarily to its thickness of 1.14 μm , which is approximately double that of S_{90C} . Multilayer structures are advantageous as they hinder crack propagation, mitigate residual stress, and facilitate the formation of highly dense microstructures. Additionally, the interfaces between layers act as barriers to boundary slipping, thereby further enhancing the hardness [30].

Figure 6 shows the scratch appearance of ta-C coating and $(Ti/ta-C)_n$ multilayer coating under the SEM. When the loading force reaches 100 N, the coating does not peel off obviously, which shows that the bonding strength of the ta-C coating and $(Ti/ta-C)_n$ multilayer coating is high and the bonding performance is excellent. As shown in Fig. 5, white debris accumulation occurs in both ta-C coating and $(Ti/ta-C)_n$ multilayer coating in the middle of scratches, which can greatly reduce the tangential force [31], thus reducing the friction coefficient of the coatings. As shown in Fig. 6a, large particles can be seen in the scratch morphology of S_{60} , indicating that the main form of wear is abrasive wear, which will negatively impact the machining quality and efficiency of coated tools. Abrasive wear is primarily influenced by a multitude of factors, including hardness differences, the presence of impurities and defects, surface roughness, coating thickness, as well as other contributing elements. Compared to other coatings, S_{60} exhibits the lowest sp^3 bond content, resulting in a reduction in the coating's hardness and wear resistance properties. This low sp^3 bond content indicates a predisposition for the coating to form a graphite structure characterized by a rough surface and large particles. Consequently, this is a contributing factor to the occurrence of severe abrasive wear. The low sp^3 bond content

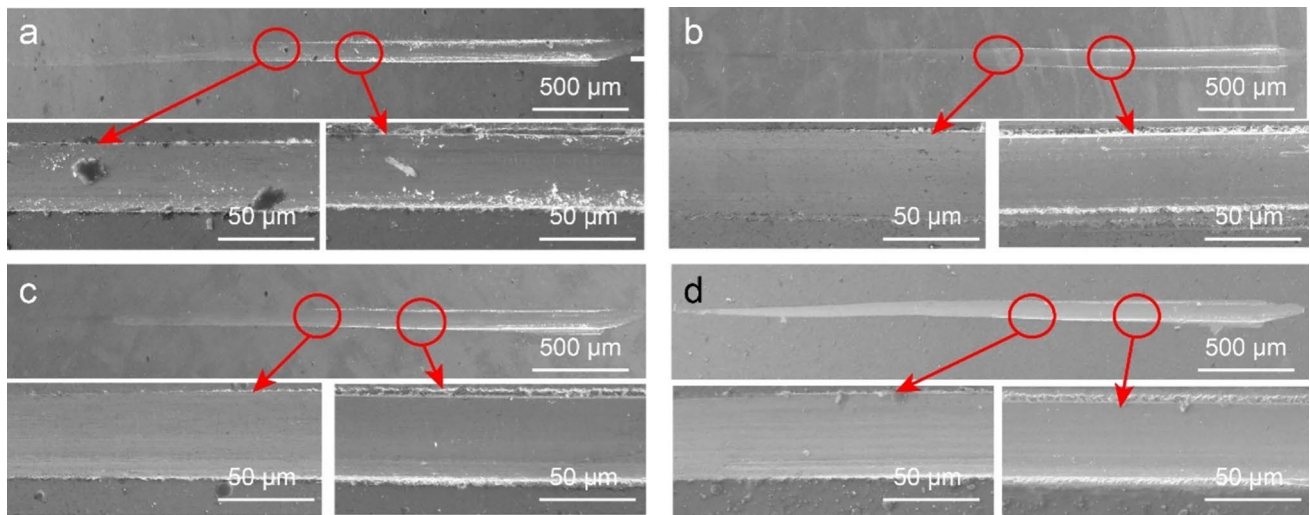


Fig. 6 Scratch morphology under SEM of ta-C coatings: **a** S_{60} , **b** S_{60C} , **c** S_{90C} , **d** $S_{120C-Ti}$

of S_{60} is mainly because of the absence of a stage cooling procedure in the preparation process, which raises the preparation temperature and causes the transformation of some sp^3 bonds to sp^2 bonds. In comparison to other coatings, the S_{60} exhibits a notably thinner thickness, predisposing it to scenarios where wear particles have an increased likelihood of directly interfacing with the coating substrate. This direct contact, in turn, exacerbates the wear process, leading to severe degradation of the coating's integrity and performance.

3.3 Tribological properties

Figure 7a displays the friction coefficient curves of ta-C coating and (Ti/ta-C) $_n$ multilayer coating. Because the surface of the coating and the friction pair are in the running-in stage in the first 600 s, and affected by the large particles on the surface, the value of the friction coefficient

will fluctuate to a certain extent, which is not stable. As the friction experiment proceeds, the friction coefficient attains relative stability, indicating the onset of the steady-state wear stage. The average value of the curve during this stage is typically adopted as the friction coefficient of the coatings, as depicted in Fig. 7b. The friction coefficients of S_{60} , S_{60C} , S_{90C} , and $S_{120C-Ti}$ are 0.079, 0.069, 0.083 and 0.087, respectively. The friction coefficient of S_{60C} is 0.069. In the course of friction interactions, a pronounced thermodynamic impetus emerges at the interfacial juncture between the coating and the mating friction partner. This impetus catalyzes the structural evolution from the initial ta-C configuration towards a graphite-like structure. As a result, a graphite-rich tribological layer with inherently low shear resistance forms, inherently functioning as an effective lubrication interface, thereby mitigating frictional forces and enhancing wear resistance [32, 33]. The friction coefficient of S_{60} is almost the same as that of S_{60C} . The

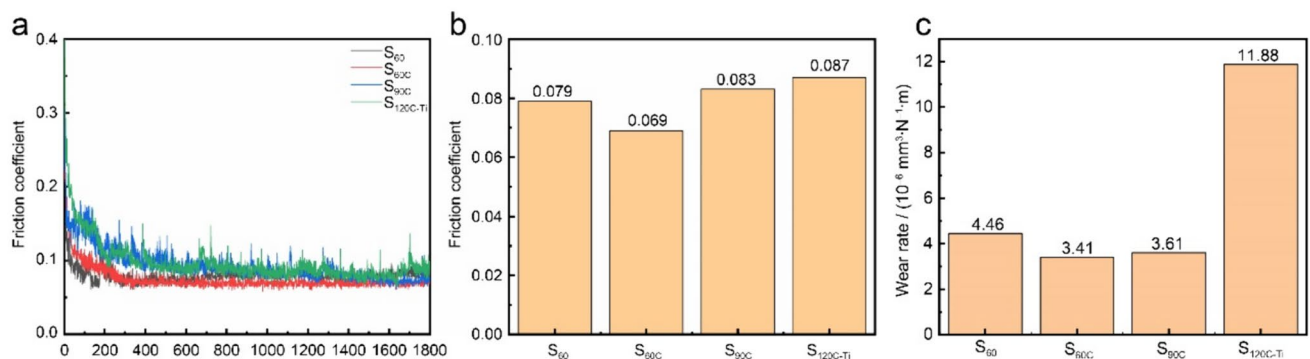


Fig. 7 Friction coefficient of ta-C coatings at **a** friction coefficient curves and **b** average friction coefficient of the coating **c** the wear rate of ta-C coatings

friction coefficient of S_{90C} and $S_{120C-Ti}$ is slightly higher, which is mainly due to the uneven surface of the coatings and the formation of larger particles on the surface. Nonetheless, the friction curves of all coatings exhibit minimal fluctuation, indicating that the friction coefficient remains stable despite variations in coating thickness and the concentration of sp^3 bonds. S_{60C} has the smallest I_D/I_G value and the lowest friction coefficient, which corresponds to the results of the previous Raman analysis in Fig. 5.

Figure 7c shows the wear rate of ta-C coatings. The graph indicates that S_{60C} exhibits the lowest wear rate of $3.4 \times 10^{-6} \text{ mm}^3 \cdot \text{N}^{-1} \cdot \text{m}^{-1}$, which is mainly due to its superior wear resistance because of its lowest I_D/I_G value and high sp^3 bond content. At the same time, S_{120-Ti} has the largest wear rate with a value of $11.88 \times 10^{-6} \text{ mm}^3 \cdot \text{N}^{-1} \cdot \text{m}^{-1}$. This is mainly due to its large I_D/I_G value, which corresponds to the structure analyzed by the coefficient of friction.

4 Conclusions

The ta-C coatings and $(\text{Ti}/\text{ta-C})_n$ multilayer coatings were prepared by arc ion plating. The results of SEM show that the interface between Ti and ta-C layer is clear. The $(\text{Ti}/\text{ta-C})_n$ multilayer structure can achieve a maximum thickness of approximately 1.14 microns, more than twice that of a directly deposited ta-C coating, significantly boosting the practical thickness limit of ta-C applications. The XRD results demonstrate an absence of distinct and pronounced diffraction peaks within the coating, indicating that the prepared coating exhibits an amorphous structure. The Raman spectra results indicate that stage cooling significantly enhances the sp^3 bond content in the ta-C coating, whereas the lower sp^3 bond content observed in $S_{120C-Ti}$ is attributed to the elevated Ti content. When the loading force reaches 100 N, the coating does not peel off obviously, which shows that the bonding strength of the ta-C coating and $(\text{Ti}/\text{ta-C})_n$ multilayer coating is high and the bonding performance is excellent. The coefficient of friction of the coating does not decrease when the thickness and content of sp^3 bonds increase and the minimum wear rate is $3.4 \times 10^{-6} \text{ mm}^3 \cdot \text{N}^{-1} \cdot \text{m}^{-1}$. The research outcomes meticulously elucidate a refined preparation technique for achieving thick ta-C coatings enriched with a substantial sp^3 bond content. This advancement significantly widens the scope of potential applications for these coatings, encompassing a broad range of tools, molds, and intricate precision engineering components.

Acknowledgements The authors acknowledge the supports of the Postgraduate Scientific Research Innovation Project of Hunan Province (No. QL20220135) and the National Natural Science Foundation of China (Nos. 12275230, 12475283 and 12027813).

Author contributions Zhi-Jun Xie: investigation, methodology, validation, writing—original draft, writing—review & editing. Jia-Lin Li: investigation, formal analysis. Ling Gong: formal analysis. Xiang-Li Zhong: supervision, methodology, funding acquisition, project administration. Hong-Jia Song: methodology, validation, writing—review & editing. Jin-Bin Wang: supervision, funding acquisition, project administration.

Data availability The data that support the findings of this study are available from the corresponding author, [hjsong@xtu.edu.cn], upon reasonable request.

Declarations

Conflict of interest The authors declare no conflict of interest.

References

1. Khan A, Nilam B, Rukhsar C, Sayali G, Mandekar B, Kadam A. A review article based on composite graphene@ tungsten oxide thin films for various applications. *Tungsten*. 2023;5(4):391. <https://doi.org/10.1007/s42864-022-00158-1>.
2. Chen G, Wang Z, Wang H, Zhao X, Hu J, Wang S, Zhang S. Effects of tetrahedral amorphous carbon film deposited on dental cobalt–chromium alloys on bacterial adhesion. *Surf Coat Technol*. 2012;206(3386):3386. <https://doi.org/10.1016/j.surfcoat.2012.01.059>.
3. Ding JC, Cheng Y, Zhang S, Wang Q, Zhang TF. Microstructure, mechanical and tribological properties of Ti-doped ta-C films deposited by a hybrid coating system. *Diamond Relat Mater*. 2023;131: 109565. <https://doi.org/10.1016/j.diamond.2022.109565>.
4. Feng KJ, Guo CQ, Lin SS, Fu ZQ, Shi Q, Su YF, Wang W, Dai MJ. Structure and properties of ta-C films prepared by vacuum cathodic arc with an unbalanced external electromagnetic field. *Ceram Int*. 2022;48(111):111. <https://doi.org/10.1016/j.ceramint.2021.09.086>.
5. Zhou HM, Jia Y, Li J, Yao SH. Corrosion and wear resistance behaviors of electroless Ni-Cu-P-TiN composite coating. *Rare Met*. 2022;41(9):3233. <https://doi.org/10.1007/s12598-015-0663-6>.
6. Komlenok MS, Arutyunyan NR, Kononenko VV, Zavedeev EV, Frolov VD, Chouprik AA, Baturin AS, Scheibe HJ, Pimenov SM. Structure and friction properties of laser-patterned amorphous carbon films. *Diamond Relat Mater*. 2016;65(69):69. <https://doi.org/10.1016/j.diamond.2016.02.006>.
7. Wei J, Guo P, Liu L, Li H, Li H, Wang S, Ke P, Wang A. Tailored electrochemical behavior of ta-C film by glancing angle deposition. *Appl Surf Sci*. 2020;516: 146115. <https://doi.org/10.1016/j.apsusc.2020.146115>.
8. Wei J, Li H, Liu L, Guo P, Ke P, Wang A. Enhanced tribological and corrosion properties of multilayer ta-C films via alternating sp^3 content. *Surf Coat Technol*. 2019;374(317):317. <https://doi.org/10.1016/j.surfcoat.2019.05.087>.
9. McKenzie DR. Tetrahedral bonding in amorphous carbon. *Rep Prog Phys*. 1996;59:1611. <https://doi.org/10.1088/0034-4885/59/12/002>.
10. Chhowalla M, Robertson J, Chen CW, Silva SRP, Davis CA, Amaratunga GAJ, Milne WI. Influence of ion energy and substrate temperature on the optical and electronic properties of tetrahedral amorphous carbon (ta-C) films. *J Appl Phys*. 1997;81(139):139. <https://doi.org/10.1063/1.364000>.

11. Hao T, Du J, Su G, Zhang P, Sun Y, Zhang J. Mechanical and cutting performance of cemented carbide tools with Cr/x/DLC composite coatings. *Int J Adv Manuf Tech.* 2020;106(5241):5241. <https://doi.org/10.1007/s00170-020-05014-5>.
12. Rajak DK, Kumar A, Behera A, Menezes PL. Diamond-like carbon (DLC) coatings: classification, properties, and applications. *Appl Sci.* 2021;11:4445. <https://doi.org/10.3390/app11104445>.
13. Wang L, Liu Y, Chen H, Wang M. Modification methods of diamond-like carbon coating and the performance in machining applications: a review. *Coatings.* 2022;12(2):224. <https://doi.org/10.3390/coatings12020224>.
14. Lei X, Wang L, Shen B, Sun F. Microdrill with variations in thickness of diamond coating. *Surf Eng.* 2016;2(165):165. <https://doi.org/10.1179/1743294414y.0000000342>.
15. Abadias G, Chason E, Keckes J, Sebastiani M, Thompson GB, Barthel E, Doll GL, Murray CE, Stoessel CH, Martinu L. Stress in thin films and coatings: current status, challenges, and prospects. *J Vac Sci Technol A.* 2018;36: 020801. <https://doi.org/10.1116/1.5011790>.
16. Gu J, Li L, Ai M, Xu Y, Xu Y, Li G, Deng D, Peng H, Luo S, Zhang P. Improvement of solid particle erosion and corrosion resistance using TiAlSiN/Cr multilayer coatings. *Surf Coat Technol.* 2020;402: 126270. <https://doi.org/10.1016/j.surfcoat.2020.126270>.
17. Dai W, Zhao XS, Cao HS, Li JL, Song HJ, Zhong XL, Wang JB. Improved thermal stability of AlCrSiN coatings base on the template effect of TiAlN layer. *Surf Eng.* 2022;38(37):37. <https://doi.org/10.1080/02670844.2021.2023389>.
18. Zha X, Wang N, Jiang F, Xu X. Performance evaluation of PVD coatings due to sequential indentation tests. *Surf Eng.* 2016;33(597):597. <https://doi.org/10.1080/02670844.2016.1161947>.
19. Zhao Z, Miao Q, Liang W, Xia J, Lin H, Qi Y, Zuo S. Effect of CrAl interlayer on adhesion strength of CrAlN coating. *Surf Eng.* 2019;36(438):438. <https://doi.org/10.1080/02670844.2019.1672956>.
20. Sui X, Liu J, Zhang S, Yang J, Hao J. Microstructure, mechanical and tribological characterization of CrN/DLC/Cr-DLC multilayer coating with improved adhesive wear resistance. *Appl Surf Sci.* 2018;439(24):24. <https://doi.org/10.1016/j.apsusc.2017.12.266>.
21. Nemati N, Penkov OV, Kim DE. Superior surface protection governed by optimized interface characteristics in WC/DLC multilayer coating. *Surf Coat Technol.* 2020;385: 125446. <https://doi.org/10.1016/j.surfcoat.2020.125446>.
22. Alimov VK, Roth J. Deuterium retention in chemically vapor deposited tungsten carbide coatings and hot-rolled tungsten exposed to low-energy deuterium plasma. *Tungsten.* 2022;4:1. <https://doi.org/10.1007/s42864-021-00120-7>.
23. Liu J, Zhang X, Zeng X, Xiong Z, Liu Y, Lei Y, Yang B. Effect of bias voltages on microstructure and mechanical properties of (AlCrNbSiTi)N high entropy alloy nitride coatings deposited by arc ion plating. *Surf Eng.* 2023;39(495):495. <https://doi.org/10.1080/02670844.2023.2236829>.
24. Wu W, Liu J, Hua T, Chen Z, Jiang J, Wang H, Liu L, Liu X. Microstructure and friction-wear behavior of multi-arc ion plating TiAlNC ceramic coating on WC-6%Co substrate. *J Mater Eng Perform.* 2018;27(9):4665. <https://doi.org/10.1007/s11665-018-3568-3>.
25. Praver S, Nugent KW, Lifshitz Y, Lempert GD, Grossman E, Kulik J, Avigal I, Kalish R. Systematic variation of the Raman spectra of DLC films as a function of sp²/sp³ composition. *Diamond Relat Mater.* 1996;5(433):433. [https://doi.org/10.1016/0925-9635\(95\)00363-0](https://doi.org/10.1016/0925-9635(95)00363-0).
26. Erdemir A, Donnet C. Tribology of diamond-like carbon films: recent progress and future prospects. *J Phys D: Appl Phys.* 2006;39:R311. <https://doi.org/10.1088/0022-3727/39/18/R01>.
27. Lin YH, Lin HD, Liu CK, Huang MW, Chen JR, Shih HC. Structure and characterization of the multilayered Ti-DLC films by FCVA. *Diamond Relat Mater.* 2010;19(1034):1034. <https://doi.org/10.1016/j.diamond.2010.02.014>.
28. Sattel S, Robertson J, Ehrhardt H. Effects of deposition temperature on the properties of hydrogenated tetrahedral amorphous carbon. *J Appl Phys.* 1997;82(4566):4566. <https://doi.org/10.1063/1.366193>.
29. Yetim AF, Kovacı H, Kasapoğlu AE, Bozkurt YB, Çelik A. Influences of Ti, Al and V metal doping on the structural, mechanical and tribological properties of DLC films. *Diamond Relat Mater.* 2021;120: 108639. <https://doi.org/10.1016/j.diamond.2021.108639>.
30. Kainz C, Schalk N, Tkadletz M, Mitterer C, Czettel C. Microstructure and mechanical properties of CVD TiN/TiBN multilayer coatings. *Surf Coat Technol.* 2019;370(311):311. <https://doi.org/10.1016/j.surfcoat.2019.04.086>.
31. Cheng YH, Browne T, Heckerman B. Mechanical and tribological properties of CrN coatings deposited by large area filtered cathodic arc. *Wear.* 2011;271(5):775. <https://doi.org/10.1016/j.wear.2011.03.011>.
32. Kong C, Guo P, Sun L, Zhou Y, Liang Y, Li X, Ke P, Lee KR, Wang A. Tribological mechanism of diamond-like carbon films induced by Ti/Al co-doping. *Surf Coat Technol.* 2018;342(167):167. <https://doi.org/10.1016/j.surfcoat.2018.02.098>.
33. Wang SL, Jiang N. Tribological performance and behavior of CVD TiC/TiCN/TiN multilayer coating at elevated temperature. *Surf Eng.* 2020;37(1):1. <https://doi.org/10.1080/02670844.2020.1807813>.

Publisher's Note Springer Nature remains neutral with regard to jurisdictional claims in published maps and institutional affiliations.

Springer Nature or its licensor (e.g. a society or other partner) holds exclusive rights to this article under a publishing agreement with the author(s) or other rightsholder(s); author self-archiving of the accepted manuscript version of this article is solely governed by the terms of such publishing agreement and applicable law.